Linear and nonlinear entropy-wave response of technically-premixed jet-flames-array and swirled flame to acoustic forcing

Author(s):
Weilenmann, Markus; Doll, Ulrich; Bombach, Rolf; Blondé, Audrey; Ebi, Dominik; Xiong, Yuan; Noiray, Nicolas

Publication date:
2021

Permanent link:
https://doi.org/10.3929/ethz-b-000452834

Originally published in:
Proceedings of the Combustion Institute 38(4), https://doi.org/10.1016/j.proci.2020.06.233

Linear and nonlinear entropy-wave response of technically-premixed jet-flames-array and swirled flame to acoustic forcing

Markus Weilenmann[a,*], Ulrich Doll[b], Rolf Bombach[b], Audrey Blondé[a], Dominik Ebi[b], Yuan Xiong[a], Nicolas Noiray[a,*]

[a] *CAPS Laboratory, Department of Mechanical and Process Engineering, ETH Zurich, Zurich 8092, Switzerland*
[b] *Paul Scherrer Institut, Forschungsstrasse 111, 5232 Villigen, Switzerland*

Abstract

Broadband combustion noise is a major part of the total noise radiated by modern jet engines. It comprises two components: *direct noise* originating from the unsteady heat release of the flame, and *indirect noise* resulting from the acceleration of entropy fluctuations in the turbine stages. Not only do these entropy waves contribute to the noise pollution of aeroengines, they can also have a crucial role in the feedback loop leading to thermoacoustic instabilities, which induce vibrations and thermal loads that are highly detrimental for combustors and turbine components. Thus, there is a critical need to understand and model the complex mechanisms associated with the generation and the advection of these waves. This study presents quantitative measurements of the production of entropy waves in a technically premixed turbulent combustor, subject to acoustic forcing. Entropy transfer function (ETF) relating acoustic input, obtained with microphones, to entropy wave output, obtained with OH-LIF thermometry at a distance of four flame heights from the burner outlet, were measured between 40 Hz and 90 Hz. These ETF were obtained using two burners of same length with technical premixing of air and natural gas, operated at the same thermal power: a matrix burner producing an array of turbulent jet flames, and a burner producing a single swirled turbulent flame. It is found that the ETF of the matrix burner exhibits a low-pass behavior, with a gain ranging from approximately 0.7 at 40 Hz down to 0.25 at 90 Hz, while the gain of the swirled flame ETF was not exceeding 0.2. It is also demonstrated that entropy wave production with the matrix burner is highly nonlinear, with a dramatic drop of the ETF gain occurring beyond a certain level of acoustic forcing amplitude. These measurements can be used to derive predictive nonlinear models of thermoacoustic instabilities involving entropy wave feedback.

Keywords: Entropy waves, Entropy transfer function, Thermoacoustic instabilities, OH-LIF Thermometry

*Corresponding authors:
Email addresses: wemarkus@ethz.ch (Markus Weilenmann), noirayn@ethz.ch (Nicolas Noiray)

1. Introduction

Decreasing temperature fluctuations and composition inhomogeneities at the outlet of aeroengine combustion chambers is becoming more and more important for the development of new combustor technologies. There are two reasons for this: First, these entropy and compositional waves contribute significantly to the noise pollution from modern aircrafts [1–3] in the form of so-called *indirect* combustion noise, which originates from the acceleration of entropy or compositional fluctuations in the turbine stages [4, 5]. Second, in the race for development of low-pollutant-emissions combustors, the manufacturers face the problem of thermoacoustic instabilities which damage the mechanical parts, and which involve constructive interaction between acoustic waves, combustion dynamics and sometimes entropy waves [6].

Entropy waves are coherent temperature fluctuations produced by unsteady combustion which are advected through the combustion chamber. As shown in this paper, they can appear when an intense acoustic field in the combustor modulates the air mass flow through the burner, which leads to equivalence ratio oscillations that transform into a modulation of the hot products temperature. If dispersion of these waves by turbulent mixing is slow with respect to the residence time of the combustion chamber, acoustic pressure fluctuations are generated when the entropy waves are accelerated in the turbine. An unstable feedback can therefore establish between combustion dynamics, entropy waves and acoustic field, and the development of new combustor technologies necessitates models to predict this type of thermoacoustic instabilities. Three major processes have to be understood: 1) The generation of entropy waves by unsteady combustion, 2) the decay of entropy waves due to shear dispersion, 3) the conversion of entropy waves to entropy noise.

Recently, studies have been performed on all 3 problems. Regarding the decay of entropy waves during advection, Eckstein et al. concluded in 2004 that in their experimental configuration, entropy waves are significantly attenuated during the advection process [7]. Recent studies aimed at deriving scaling laws for the spatial decay of the entropy waves, [8–11] but most of them considered very simplified configurations, which calls for further investigations with turbulent reacting flows in complex geometries that are relevant for practical systems. Studies that focus on the conversion of entropy waves to entropy noise [12–14] usually rely on synthetically generated temperature waves, using, for instance, electric heaters. Recently, several numerical and experimental studies dealing with the production of entropy waves, were conducted [15–20]. However, there is still a compelling need for further experimental data, especially with turbulent technically premixed flames under technical premixing of fuel and air, for which temperature fluctuation measurements are very challenging. This study aims to contribute to fill this gap with quantitative temperature measurements by OH-PLIF thermometry [21]. The next section describes the combustor and the diagnostics used in this study. Section 3 provides information on the methods for postprocessing the acoustic and optical data. Section 4 presents the entropy transfer function (ETF) measured for an array of turbulent jet flames and for a single turbulent swirled flame at low and high forcing amplitudes.

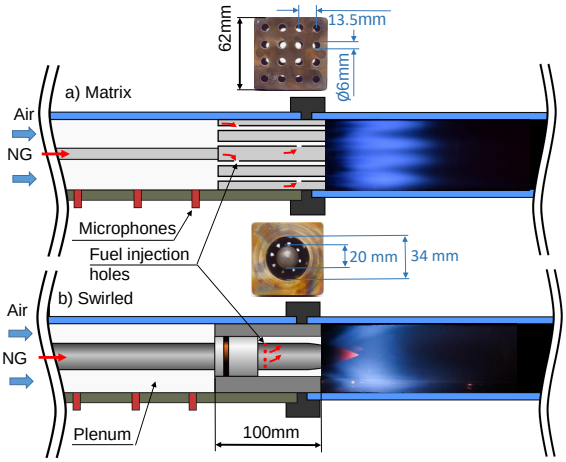

Figure 1: Sketches of the generic combustor equipped with a) the matrix burner, and with b) the axial-swirler burner. Pictures and main dimensions of the burners are shown. Stiff-injection of the natural gas (NG) in the air flow is done inside the burners (technical premixing).

2. Experimental Setup

2.1. Test rig

The experiments were conducted with a modular combustor operated at atmospheric pressure (see Fig. 1). It consists of a plenum and a combustion chamber (62×62 mm^2 cross section) terminated by an orifice plate to ensure thermo-acoustically stable operation for all the conditions considered in this work. Exchangeable side walls for optical access (quartz windows), or instrumentation (ceramic or water-cooled aluminium plates with microphone ports, hot gas probe, igniter, etc) are mounted on a water-cooled aluminium frame made of a series of 250 mm long modules. The plenum features an acoustically stiff main air injection and sealed loudspeaker modules that are connected to the plenum

with ceramic honeycombs. Natural gas is either directly injected with the air into the plenum in order to achieve perfectly premixed conditions at the burner inlet, or within the burner for technical premixing. Three microphones (G.R.A.S. 46BD-S2) were placed between the loudspeakers module and the burner to measure forward and backward acoustic travelling waves.

Two burners of 10 cm length were considered: a matrix burner shown in Fig. 1a featuring 4×4 channels producing 16 turbulent jet flames, and a burner with an axial swirler producing a single swirled turbulent flame which is depicted in Fig. 1b. The matrix burner made of Hastelloy X was additively manufactured with selective laser melting to form a hollow cavity from which natural gas is injected via 16 small holes (one per channel) of diameter 0.8 mm in order to achieve acoustically stiff injection at nominal condition. The holes are axially staged (8 at 70 mm and 8 at 20 mm from the burner outlet) for improved thermoacoustic stability. The gas injection holes staging distance was defined in the same way as the vortex generators staging in [22]. The second burner features a central lance (⌀20 mm) with an axial swirler, inserted in a hole (⌀34 mm) in order to form an annular channel. The lance is terminated by an ogive shaped tip protruding into the combustion chamber. The 8 fuel injection holes are evenly spread around the circumference 20 mm downstream of the swirler at the same axial position. The nominal conditions of 30 kW thermal power and equivalence ratio $\phi = 0.76$, were maintained throughout the study with the exception of the experiments investigating the effect of ϕ and the comparison between technically and perfectly premixed conditions. For the latter, the thermal power was increased to 40 kW, because stable operation was not possible at 30 kW under perfectly premixed conditions. The first module of the combustion chamber is equipped with 4 quartz windows, which provides optical access to the flame and identical heat losses on the four sides. A ceramic plate equipped with an electric igniter and three quartz windows are mounted as side walls of the second module of the combustion chamber such that OH-PLIF in the hot products could be performed (see Fig.2).

2.2. OH PLIF-thermometry and chemiluminescence

Planar temperature distributions downstream of the combustion chamber for the matrix as well as the axial-swirler burner configuration were acquired by means of simultaneous OH-PLIF and OH laser absorption measurements [21]. By combining both methods, the local, instantaneous OH concentration can be determined from a single laser pulse. The laser light absorption measurement is used for both the absorption correction

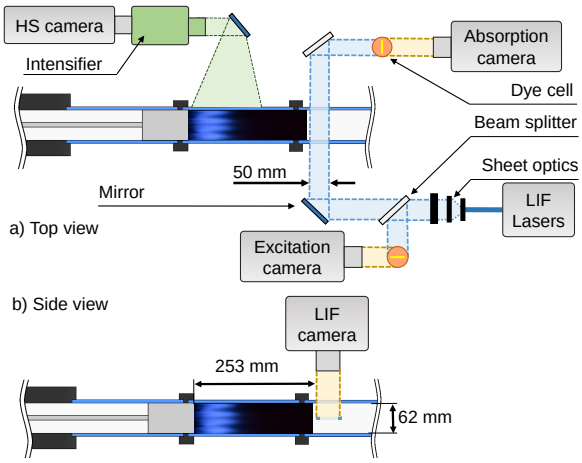

Figure 2: Schematical arrangement of the optical components and cameras used for combined OH-PLIF/OH absorption thermometry and OH chemiluminescence measurements of the flame.

of the LIF images as well as the absolute calibration of the OH concentration. By assuming chemical equilibrium in the hot products and under lean conditions ($\phi < 0.9$), the resulting single-pulse OH concentration field is almost independent of the equivalence ratio [21] and, therefore, can unambiguously be converted into an instantaneous temperature distribution. Due to the rapid decrease of OH concentration with temperature, the method has a lower temperature detection limit of approximately 1300 K. Taking into account the accuracy considerations summarized in [21], the measurement uncertainty of the method is below 5 % in the observed temperature range of 1600 K to 2100 K. Recently, the technique has been sucessfully applied to measure planar temperature distributions in high pressure combustion environments related to aeroengine [23] and stationary gas turbine research [24]. In Figure 2, the optical setup of the combined OH-PLIF/OH absorption measurements is depicted. The LIF signal was excited using a frequency-doubled dye laser (Quantel TDL 90 pumped with YG981, ~ 20 mJ per pulse at 20 Hz, 0.08 cm^{-1} FWHM) tuned to the $Q_1(8)$ transition of the A-X ($v' = 1, v'' = 0$) band near 283.55 nm. The laser beam was formed into a collimated light sheet by using a combination of cylindrical lenses ($f = -25$ mm, $f = 400$ mm). To avoid saturation effects on the OH fluorescence signal, the resulting sheet width was twice as large as required and only the central 45 mm were used for the measurements. Likewise, the pulse energy was attenuated to about 50 % and a third cylindrical lens ($f = 1000$ mm) was used to position the beam waist outside the test section. The resulting sheet thickness

was of the order of 1 mm throughout the imaged domain. Prior to the actual experimental campaign, LIF saturation was investigated in a matrix burner laboratory experiment ($\phi = 0.8$), using the same light sheet and signal collection optics. Images of the OH-PLIF signal were acquired at pulse energies of 100 %, 50 % and 25 % and OH concentrations as well as temperatures were derived. A saturation effect was observed for the unattenuated beam, whereas the curves for 50 % and 25 % converged to similar values. Due to the higher signal to noise ratio, the 50 % setting is used in the measurements. The OH-fluorescence emission from the horizontally oriented sheet was captured from above with an intensified CCD camera (PCO Dicam Pro), equipped with an UV lens (Cerco, 100 mm f/2.8) and a bandpass interference filter (Chroma, T > 70 % at 310 nm, FWHM 10 nm). The resulting camera field-of-view was 62×62 mm^2 at a spatial resolution of 120 μm per pixel. To perform the simultaneous measurement of OH laser light absorption, part of the incoming and outgoing light sheet was deflected by beam splitters onto two cuvettes filled with dye solution. The resulting intensity profiles before and behind the test section were recorded with two CCD cameras of the same type (PCO Pixelfly equipped with Schneider-Kreuznach 25mm f/.95 lens). The cameras were synchronized at 10 Hz to capture every second light pulse. To resolve the fast coherent oscillations of hot gas temperature in response to the acoustic forcing imposed with the loudspeaker (40 – 90 Hz), phase-locked averaging was performed by synchronizing the onset of the forcing sinusoidal signal with the 10 Hz acquisition rate of the PLIF system. For excitation frequencies being integer multiples of 10 Hz, phase-sweeps of the loudspeaker forcing could then be performed by merely modifying the phase of their input signal. While this approach results in very accurate phase-locking, it is also very time consuming, because the data has to be measured, stored and processed at each phase angle separately. Convergence of the spatially integrated phase-locked averaged temperature fields within one percent was reached after 100 cycles, by which we mean that the addition of the 101st cycle changed the result by less than 1 %.

High speed OH* chemiluminescence of the flame was recorded using a highspeed camera (Photron HSSX) and a highspeed intensifier (Lavision highspeed IRO), as depicted in Fig. 2 a). A UV lens (Cerco, 100 mm f/2.8) was used together with an optical narrow bandwidth (10 nm) filter centered around 308 nm. Due to space limitations, the camera setup was mounted parallel to the test rig and a UV mirror was used to observe the flame.

3. Methodology

The goal of this paper is to investigate the entropy wave generation by an array of 4×4 turbulent jet flames and by a single turbulent swirled flame, which are operated at the same thermal power and equivalence ratio with technical premixing of air and NG, when they are submitted to an acoustic forcing. To that end, we consider the single input/ single output (SISO) Entropy Transfer Function (ETF), which relates the coherent velocity fluctuations u' just upstream of the burners to the coherent averaged temperature fluctuations T' at a distance of 4 flame heights from the burners outlet, where $\bar{u}$ and $\bar{T}$ represent the mean absolute axial velocity and temperature:

$$ETF = \frac{T'/\bar{T}}{u'/\bar{u}} \tag{1}$$

These positions for the measurements of mean and oscillating velocity and temperature were chosen for the following reasons: First, the length of the burners $L_\mathrm{b} = 0.1$ m is small compared to the shortest acoustic wavelength considered in this work ($\lambda_\mathrm{min} = c/f_\mathrm{max} = 340/120 = 2.8$ m), and one can expect a quasi-incompressible motion of the air in the compact burner where $u'/\bar{u}$ just upstream of the burner inlet is the same as $u'/\bar{u}$ at the axial position of the NG holes. Second, the quantitative measurement of temperature using LIF thermometry requires the mixture to be at equilibrium, which is not the case in the direct vicinity of the flame, and which motivated our decision to measure the temperature field significantly downstream of the flame, in the second combustion chamber module.

3.1. Quantification of acoustic velocity

The acoustic velocity at the inlet of the matrix is reconstructed from the pressure signals of the three microphones placed upstream of the burner using the Multi-Microphone Method. With this method, the acoustic pressure is expressed as the solution of the one-dimensional wave equation with mean flow:

$$\hat{p}(\omega, x) = \hat{f}(\omega) e^{-i\frac{\omega}{c}\frac{x}{1+M}} + \hat{g}(\omega) e^{i\frac{\omega}{c}\frac{x}{1-M}} \tag{2}$$

where $\hat{\cdot}$ denotes the Laplace transformation, and where the Riemann invariants $\hat{f}$ and $\hat{g}$ are determined from an overdetermined system using least-square inversion [25]. The acoustic velocity $\hat{u}(\omega)$ at the burner inlet is then reconstructed as $\hat{u}(\omega) = \rho c(\hat{f}(\omega) - \hat{g}(\omega))$. The mean flow velocity $\bar{u}$ is determined from the air mass flow measurement and the plenum cross section area ($62 \times 62 - \pi \times 10^2/4 = 3765$ mm^2) using a Bronkhorst mass flow meter.

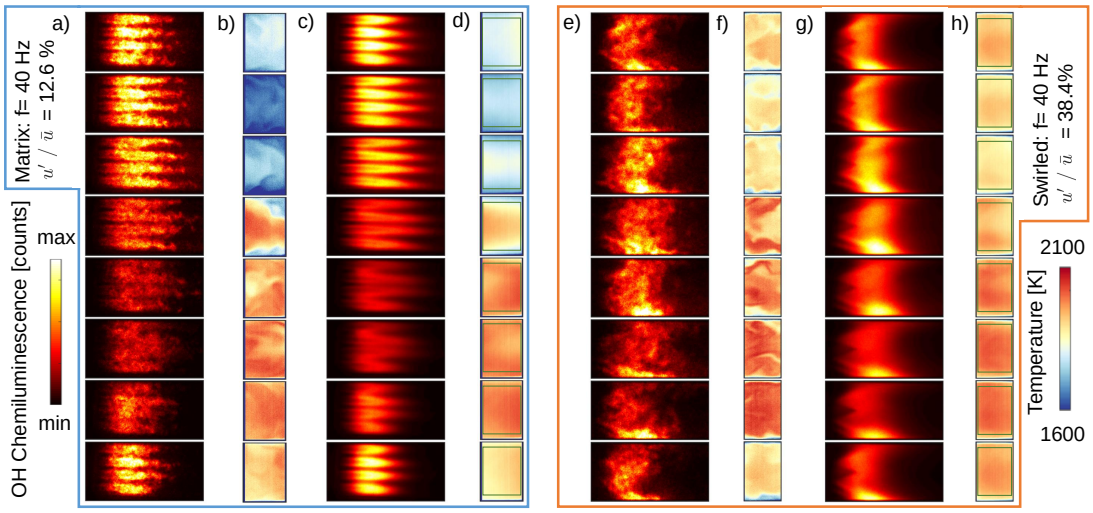

Figure 3: OH* Chemiluminescence (OH CHEM) and LIF thermometry at a forcing frequency of 40Hz for the configurations with matrix burner (a-d) and for the burner with swirler (e-h).. a,e) Instantaneous OH CHEM ; b,f) instantaneous LIF results; c,g) phase-averaged OH CHEM d,h) phase-averaged LIF results. The green rectangles show the ROI at 40 Hz.

3.2. Thermometry and chemiluminescence

The high-speed OH chemiluminescence recordings of both flame types showed significant fluctuation in intensity and flame length. Using the purely sinusoidal loudspeaker excitation signal as a reference, a phase angle was assigned to each recorded frame. The high frame-rate allows the observation of instaneous cycles, as shown in Figure 3a (matrix) and 3e (swirled) for an excitation frequency of 40 Hz for both the matrix and swirled type flame. By phase binning and subsequent phase-averaging, columns 3c and 3g are obtained, showing the coherent fluctuation in OH chemiluminescence intensity, which can serve as an indication for heat release rate fluctuation. A larger amplitude is evident for the jet flames of the matrix burner in this case.

The combined OH-PLIF/OH absorption measurements provide instantaneous snapshots of the absolute temperature distribution in the light sheet. The 10 Hz TTL signal for the OH-PLIF was used as reference for the generation of the acoustic excitation signals. By introducing a phase shift to the acoustic excitation signal several phase angles at the same operating condition were captured. Figures 3b and 3f show such instantaneous results for 8 phase angles at a forcing frequency of 40 Hz for the matrix burner and the one with swirler. Columns d and h show the coherent fluctuation obtained by averaging over 120 cycles at a constant phase angle. To further process these phase averaged planar temperature fields, a region of interest (ROI) was selected in the center of the fields, as shown in Fig. 3d and 3h, to extract a scalar average for each phase angle. The very

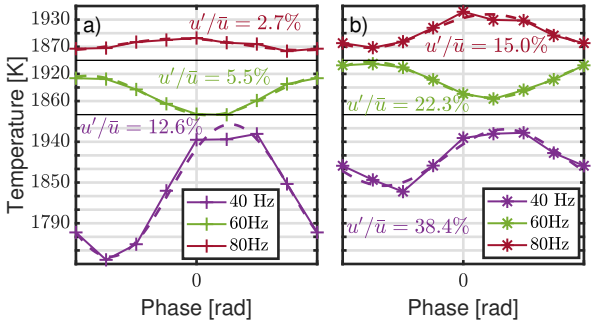

Figure 4: Phase-averaged spatial averages within ROI of OH-PLIF thermometry data measured downstream of the matrix (a) and swirl (b) burners, with corresponding Fourier component.

top and bottom regions of the temperature fields were excluded to remove the cold boundary layer of the wall. The width of the ROI was chosen to be 1/16 of the expected entropy wave wavelength. The spatial average of the temperature values within this ROI was then used for further processing. Figure 4 shows the evolution over one phase-averaged cycle for 3 selected frequencies and both burner types. The quantity of interest here is the fluctuation amplitude taken as the Fourier coefficient at the forcing frequency.

4. Results and discussion

4.1. Perfectly premixed vs technically premixed

In order to confirm that equivalence ratio fluctuations are the dominant source of coherent entropy fluctua-

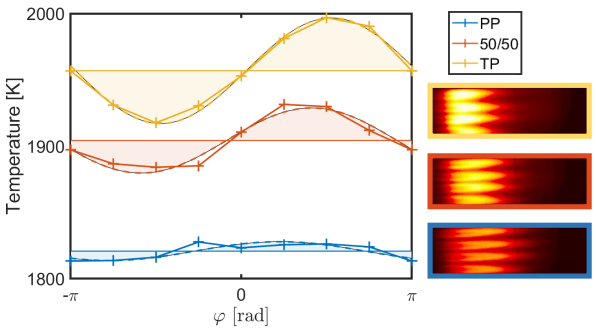

Figure 5: Hot gas temperature averaged in the ROI downstream of the jet flames of the matrix burner obtained by OH-PLIF thermometry. The acoustic forcing of the flames was performed at 60 Hz for perfectly premixed and technically premixed conditions (40 kW thermal power and ϕ=0.76). The OH* chemiluminescence images of the flames are averages of 1000 snapshots without acoustic forcing.

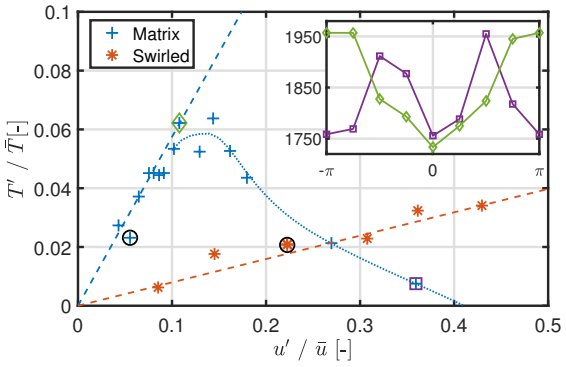

Figure 6: Amplitude of the coherent temperature response at the forcing frequency (60 Hz) measured by OH-LIF thermometry as a function of acoustic velocity fluctuation amplitude upstream of the burner. 30kW thermal power at ϕ=0.76. The inset shows the temporal evolution of phase-averaged temperature measurements for the data points marked in green and violet. Black circles mark data sets also shown in Fig. 8.

tions in this work, perfectly premixed conditions, where the fuel was injected close to the main air inlet, are compared to technically premixed conditions, where the fuel was injected using the fuel injection holes shown in Fig. 1. The obtained phase-averaged temperature values and resulting Fourier component at forcing frequency are presented in Fig. 5. A clear decrease in temperature oscillation amplitude is observed, when comparing the perfectly premixed (PP) dynamics to the technically premixed (TP) one. This was expected because in perfectly premixed conditions, the acoustic forcing does not induce equivalence ratio modulation. In the case of the 50/50 NG mass flow split between the two gas lines, the amplitude of the equivalence ratio fluctuations is reduced accordingly, which explains the measured intermediate temperature fluctuation amplitude. Figure 5 also depicts OH chemiluminescence images of the unforced flames. The technically premixed case looks more compact at first glance, but if lower intensity areas downstream of the flame are considered as well, it is less compact than the perfectly premixed flame. With a single gas injection hole per channel, ϕ can exhibit a certain degree of stratification at the outlet of the matrix channels, giving rise to turbulent jet flames with a lean faint side that extends further downstream than the rich bright side. This is consistent with the higher mean temperature measured in the planar ROI for the technically premixed flame, although the thermal power and global equivalence ratio were identical in all 3 cases. This observation may be explained also by flamelets burning richer mixtures than the global equivalence ratio because of technical premixing and that the resulting local hot spots have not mixed sufficiently with the colder regions of the flow in the laser sheet plane at the ROI.

4.2. Nonlinearities at high forcing amplitude

Measurements were performed at increasing forcing acoustic amplitude in order to assess the nonlinearities in the the entropy-wave response of the array of jet flames and of the swirled flame at f = 60 Hz. The operating condition was kept constant at 30kW thermal power and ϕ=0.76. The results presented in Fig. 6 show a much steeper linear trend, and therefore higher gain, for the matrix burner than for the one with swirler.

In the matrix burner case, a substantial drop of the temperature oscillation amplitude at the forcing frequency is observed for acoustic velocity amplitudes at the burner inlet that exceed 10% of the mean velocity. This strong nonlinearity leads to a sudden decrease of the ETF gain, as shown in Fig. 7a. The temperature oscillation amplitude almost vanishes for acoustic forcing higher than 30 % because coherent response at the forcing frequency only is considered, as explained in Section 3. However, in the non linear regime, response energy is transferred to multiples of the forcing frequency, and primarily to the first harmonic, as illustrated in Fig. 6 for the data points indicated by the green diamond and the violet square. In contrast, the significantly weaker response of the swirled turbulent flame does not display any clear nonlinear regime, even for acoustic velocity forcing amplitudes that exceed 40% of the mean flow velocity. The instantaneous OH* chemiluminescence images presented in Fig. 7b, show a clear difference in flame dynamics between the flames forced

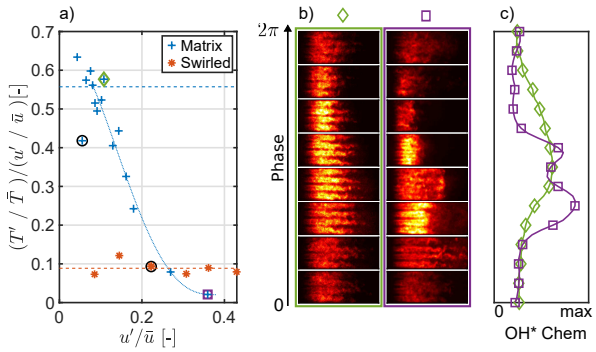

Figure 7: a) Gain as a function of forcing amplitude at f = 60Hz. Black circles indicate data shown in Fig. 8. b) Instantaneous snapshots of OH* Chemiluminescence (8 phase angles) for a point in the linear regime (green diamond) and in the non-linear regime (violet square). c) Integrated OH* Chemiluminescence

in the linear and non-linear regimes. The corresponding integrated values, shown in Fig. 7c, show the split of energy to other frequencies, already observed in Fig. 6. The velocity fluctuations may be responsible for further spreading of the energy during advection. The black circles in Figs. 6 and 7 indicate the data points used to deduce the ETF in Section 4.3. This data was obtained on a different date, which explains the observable discrepancies for two reasons. The environmental boundary conditions, like pressure and humidity, vary daily and the tests were performed using natural gas supplied by the municipal authority, which varies slightly in composition from day to day.

4.3. Entropy transfer function

The ETF measurements were performed by imposing, for a range of frequencies, a forcing leading to a constant acoustic pressure amplitude at the flame, which was accompanied by significant variations of the normalized acoustic velocity. In the case of the matrix burner, the forcing amplitude of the acoustic velocity was kept below the response-nonlinearity threshold in order to provide the ETF. However, for the burner with swirl, it was necessary to impose a significantly higher forcing level to obtain a similar response amplitude as shown in Fig. 4. The acoustic input, temperature output and resulting ETF are plotted on Fig. 8. One can clearly see the significantly higher gains of the matrix-burner compared to the swirler. The matrix-burner ETF exhibits the expected low-pass filter behavior, also observed in [18] for similar Strouhal numbers. This behavior is not observed for the gain curve of the burner with swirler, which may be explained by the fact that it was obtained by forcing at significantly higher amplitudes.

Still, from Fig. 6 and 8, one can make the general conclusion that matrix-type burners exhibit ETF with significantly higher gains than burners with swirler and are therefore more prone to low-frequency instabilities involving constructive coupling between acoustics, flames and entropy-waves. This is due to the faster mixing of the temperature fluctuations in the swirling flow (e.g. [26]) which leads to a very fast decay of spatially integrated coherent temperature fluctuations.

Figure 8d shows the gain between the acoustic velocity forcing and the entropy-wave amplitude output for increasing global equivalence ratio but constant thermal power of 30kW and constant excitation frequency of 60 Hz. The significant difference in gain between matrix and burner with swirler is consistent with the previous observations shown in Fig. 8c. With the exception of a minor anomaly around ϕ=0.71, a decreasing trend in gain is observed in both cases for richer mixtures.

5. Conclusions

Temperature waves originating from two types of acoustically forced flames were successfully measured by simultaneous OH-PLIF and OH absorption measurements. The equivalence ratio oscillations caused by acoustic velocity forcing were identified to be the dominant source of entropy wave generation in technically premixed conditions. Entropy transfer functions (ETF) were deduced from these measurements. It was demonstrated that the matrix burner response is strongly nonlinear for acoustic velocity forcing amplitudes exceeding 10% of the mean flow velocity due to a sudden transition from a response at the fundamental frequency to a response at twice the forcing frequency. It is also found that for same forcing amplitudes, the swirled flame produces much weaker entropy waves than the array of jet flames because of enhanced turbulent mixing from the swirling flow, which was expected. It suggests that the matrix-type burner promotes thermoacoustic instabilities involving low-frequency entropy-wave feedback in short combustors exhibiting low residence time.

References

[1] A. P. Dowling, Y. Mahmoudi, Combustion noise, Proceedings of the Combustion Institute 35 (2015) 65 – 100.

[2] A. S. Morgans, I. Duran, Entropy noise: A review of theory, progress and challenges, International Journal of Spray and Combustion Dynamics 8 (2016) 285–298.

[3] M. Ihme, Combustion and engine-core noise, Annual Review of Fluid Mechanics 49 (2017) 277–310. Cited By 33.

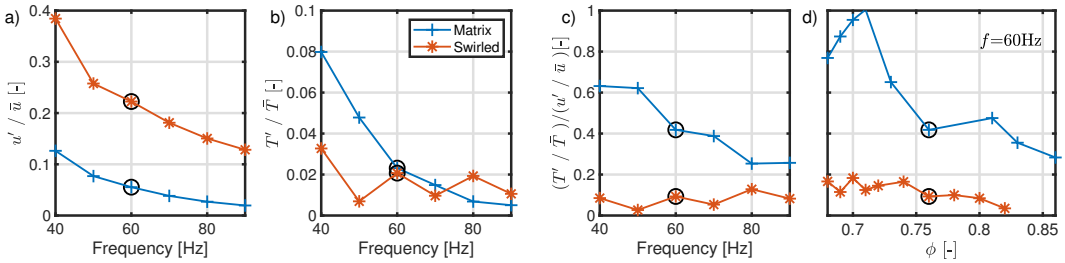

Figure 8: a) Reconstructed acoustic velocity at the inlet plane of the burner of the burners. b) Temperature fluctuation amplitudes at the forcing frequency extracted from OH-LIF thermometry fields. c) Resulting ETF gain between acoustic input and entropy output for matrix and swirled burner. All tests in a), b) and c) were conducted at 30 kW thermal power and ϕ=0.76. The presented frequency range results in Strouhal numbers between $St \approx 0.5$ to 1.2. d) ETF Gain between normalized acoustic velocity input and temperature modulation output for varying global ϕ at 30 kW and f = 60 Hz. Data points also shown in Fig. 6 are marked by black circles.

[4] F. Marble, S. Candel, Acoustic disturbance from gas non-uniformities convected through a nozzle, Journal of Sound and Vibration 55 (1977) 225 – 243.

[5] L. Magri, J. O'Brien, M. Ihme, Compositional inhomogeneities as a source of indirect combustion noise, Journal of Fluid Mechanics 799 (2016). Cited By 28.

[6] T. Poinsot, Prediction and control of combustion instabilities in real engines, Proceedings of the Combustion Institute 36 (2017) 1 – 28.

[7] J. Eckstein, E. Freitag, C. Hirsch, T. Sattelmayer, Experimental study on the role of entropy waves in low-frequency oscillations for a diffusion burner, Proceedings of the ASME Turbo Expo (2004) 743–751.

[8] A. S. Morgans, C. S. Goh, J. A. Dahan, The dissipation and shear dispersion of entropy waves in combustor thermoacoustics, Journal of Fluid Mechanics 733 (2013).

[9] A. Giusti, N. A. Worth, E. Mastorakos, A. P. Dowling, Experimental and numerical investigation into the propagation of entropy waves, AIAA Journal 55 (2017) 446–458.

[10] Y. Mahmoudi, A. Giusti, E. Mastorakos, A. P. Dowling, Low-Order Modeling of Combustion Noise in an Aero-Engine: The Effect of Entropy Dispersion, Journal of Engineering for Gas Turbines and Power 140 (2017).

[11] Y. Xia, I. Duran, A. S. Morgans, X. Han, Dispersion of entropy perturbations transporting through an industrial gas turbine combustor, Flow, Turbulence and Combustion 100 (2018) 481–502.

[12] F. D. Domenico, E. O. Rolland, S. Hochgreb, A generalised model for acoustic and entropic transfer function of nozzles with losses, Journal of Sound and Vibration 440 (2019) 212 – 230.

[13] F. D. Domenico, E. O. Rolland, S. Hochgreb, Detection of direct and indirect noise generated by synthetic hot spots in a duct, Journal of Sound and Vibration 394 (2017) 220 – 236.

[14] F. Bake, C. Richter, B. Mhlbauer, N. Kings, I. Rhle, F. Thiele, B. Noll, The entropy wave generator (ewg): A reference case on entropy noise, Journal of Sound and Vibration 326 (2009) 574 – 598.

[15] B. Semlitsch, T. Hynes, I. Langella, N. Swaminathan, A. P. Dowling, Entropy and vorticity wave generation in realistic gas turbine combustors, Journal of Propulsion and Power 35 (2019) 839–849.

[16] G. Wang, X. Liu, S. Wang, L. Li, F. Qi, Experimental investigation of entropy waves generated from acoustically excited premixed swirling flame, Combustion and Flame 204 (2019) 85 – 102.

[17] R. Bluemner, C. O. Paschereit, K. Oberleithner, Generation and transport of equivalence ratio fluctuations in an acoustically forced swirl burner, Combustion and Flame 209 (2019) 99 – 116.

[18] T. Steinbacher, M. Meindl, W. Polifke, Modelling the generation of temperature inhomogeneities by a premixed flame, International Journal of Spray and Combustion Dynamics 10 (2018) 111–130.

[19] L. S. Chen, S. Bomberg, W. Polifke, Propagation and generation of acoustic and entropy waves across a moving flame front, Combustion and Flame 166 (2016) 170 – 180.

[20] Y. Sun, D. Zhao, S. Ni, T. David, Y. Zhang, Entropy and flame transfer function analysis of a hydrogen-fueled diffusion flame in a longitudinal combustor, Energy 194 (2020) 116870.

[21] J. Heinze, U. Meier, T. Behrendt, C. Willert, K.-P. Geigle, O. Lammel, R. Lckerath, Plif thermometry based on measurements of absolute concentrations of the oh radical, Zeitschrift fr Physikalische Chemie 225 (2011) 1315–1341.

[22] N. Noiray, D. Durox, T. Schuller, S. Candel, Dynamic phase converter for passive control of combustion instabilities, Proceeding of the Combustion Institute 32 (2009) 3163–3170.

[23] U. Doll, G. Stockhausen, J. Heinze, U. Meier, C. Hassa, I. Bagchi, Temperature Measurements at the Outlet of a Lean Burn Single-Sector Combustor by Laser Optical Methods, Journal of Engineering for Gas Turbines and Power 139 (2016). 021507.

[24] M. Severin, O. Lammel, H. Ax, R. Lckerath, W. Meier, M. Aigner, J. Heinze, High Momentum Jet Flames at Elevated Pressure: Detailed Investigation of Flame Stabilization With Simultaneous Particle Image Velocimetry and OH-LIF, Journal of Engineering for Gas Turbines and Power 140 (2017). 041508.

[25] B. Schuermans, Modelling and Control of Thermoacoustic Instabilities, Thesis, EPFL, 2003.

[26] O. Tammisola, M. P. Juniper, Coherent structures in a swirl injector at re =4800 by nonlinear simulations and linear global modes, Journal of Fluid Mechanics 792 (2016) 620657.